Magnetically tightened form-stable phase change materials with modular assembly and geometric conformality features

Yongyu Lu
Chinese Academy of Sciences
Dehai Yu
China Agricultural University
Haoxuan Dong
China Agricultural University
Jinran Lv
China Agricultural University
Lichen Wang
Chinese Academy of Sciences
He Zhou
University of Science and Technology Beijing
Jing Liu
Chinese Academy of Sciences & Tsinghua University
Zhi-Zhu He (zzhe@cau.edu.cn)
China Agricultural University

Article

Keywords: phase change materials, magnetism, energy storage

Posted Date: October 13th, 2021

DOI: https://doi.org/10.21203/rs.3.rs-948120/v1

Version of Record: A version of this preprint was published at Nature Communications on March 16th, 2022. See the published version at https://doi.org/10.1038/s41467-022-29090-1.

Abstract

Recently, phase change materials (PCMs) have attracted significant attention due to their promising applications in many fields like solar energy and chip cooling. However, the present PCMs seriously suffer inevitable leakage and low thermal conduction. Magnetism can produce invisible field effects in the surrounding space. If there exist magnetic particles within this region, the effects will act on them emerging various fascinating phenomena. Inspired by this, we introduce hard magnetic particles (which can keep the effect after removing the magnetic field) to PCMs synthesizing an unprecedented magnetically tightened form-stable PCMs (MTPCMs), achieving multifunctions of leakage-proof, dynamic assembly and morphological reconfiguration, superior high thermal (increasing of 1400%~1600%) and electrical (>10^4 S/m) conductivity, and prominent compressive strength. Novel free-standing temperature control and high-performance thermal and electric conversion systems based on MTPCMs are furthermore developed. This work is a significant step toward exploiting a smart PCM for electronics and low-temperature energy storage.

Introduction

Phase change materials (PCMs) are such a class of materials that absorb or release large amounts of heat while their temperature keeps constant during the melting or solidifying process. In thermal energy storage (TES) systems, latent heat storage has distinct advantages over sensible heat storage or thermochemical reactions due to its high energy density with a slight temperature swing[1, 2, 3]. PCMs play a vital role in the latent heat storage technique, and PCMs based latent heat storage is regarded as a promising technology to cope with energy and environmental crisis and thus has been extensively studied in recent years[4, 5, 6]. The research results demonstrate that PCMs have great potentials in areas like solar energy, load shifting/leveling, and waste heat recovery[7]. They alleviate the discontinuous and intermittent nature of solar irradiation and offset the mismatch between electricity supply and demand[8, 9]. In addition, practical applications of PCMs are constantly widened ranging from electronic cooling, green buildings, smart textiles to infrared stealth with the deepening of research[10].

Despite the great progress that has been made in developing PCMs, their performance still exists several shortcomings, including low thermal conductivity, liquid leakage, supercooling, and phase separation[4]. Although supercooling and phase separation behaviors deteriorate the storage capacity and thermal stability of PCMs, these two behaviors only occur in hydrate salts[11]. The common and critical bottlenecks of PCMs are their low thermal conductivity and leakage issue[2, 4, 12, 13, 14]. Inherent low thermal conductivity limits the heat transfer within PCMs and consequently results in the reduction of thermal diffusion rate. The main way to solve this problem is incorporating metal-, carbon- or ceramic-based high-thermal-conductivity additives into PCMs matrix[1, 2, 4]. Compared with thermal conductivity, liquid leakage is a more troublesome agenda that is worth concentrating on, as fluid PCMs can lead to contamination, corrosion, or even short circuit of equipment. Considerable work has been dedicated to tackling this issue, such as encapsulating PCMs with shells to produce core-shell-like capsules[15, 16]. However, the shell

usually presents a weak thermal response and influences the thermophysical properties of PCMs, and they exist the risk of rupture under large thermal stress[17]. More importantly, though adding high thermal conductivity materials and PCMs encapsulation can compensate for the abovementioned defects of PCMs, introducing excessive additives sacrifices their energy storage density. In this case, employing three-dimensional (3D) structural substances with high thermal conductivity to make form-stable PCMs becomes the focus of research[4]. The 3D structural substances act as not only the thermal conductivity promoter but also supporting materials, which significantly decreases the filler loading of PCMs. Among these substances, 3D carbon materials and metal foams are the most frequently used additives[18, 19, 20]. Carbon materials generally exhibit low dimensional morphology. It is particularly difficult for them to construct an interconnected thermal conduction framework, and the resulting materials often present extremely low thermal conductivity due to the loose contact, which means the increase in thermal conductivity of the as-prepared form-stable PCMs is very limited[21, 22]. As for metal foams, it is not easy to impregnate PCMs into their inner pores and obtain thoroughly filled composites because of the large surface tension or insufficient wetting of PCMs to the metal[19]. Up to now, the effective method to synthesize form-stable PCMs is still lacking and further explorations are in demand.

Applying an external magnetic field, hard magnetic particles agglomerate together forming a 3D cluster with abundant interparticle pores and such structure can keep intact after removing the magnetic field. Inspired by this phenomenon, we introduce hard magnetic particles as the supporting material into PCMs. Under the capillary action, liquid PCMs fill inner micropores forming liquid bridges and then be stabilized inside the magnetic cluster, which enables PCMs to be leakage-proof. This is an original idea to synthesis form-stable PCMs, here as a proof of concept, we select NdFeB and paraffin, the most commonly used hard magnetic material and organic PCM, as the input for our system. NdFeB particles are surface modified to NdFeB@Ag through in situ silver-plating to improve their thermal conductivity. Different from conventional supporting materials which must possess or build a prerequisite 3D structure, NdFeB@Ag particles can directly mix with paraffin like general particles, in the following magnetization process, they align along the magnetic field constructing an oriented network thereby fabricating a magnetically tightened form-stable phase change material (MTPCM), as illustrated in Fig. 1a. Our approach ensures saturated filling of PCMs between tightly connected NdFeB@Ag particles, eliminating the universal incomplete filling and incompact contact problems in form-stable PCMs. It needs to be emphasized that the 3D structure made of magnetic-oriented hard magnetic particles is the core of MTPCMs. It endows MTPCMs with a robust structure and magnetism. As a result, they not only demonstrate the leakage-proof ability and shape stability during the phase change process but also exhibit magnetic assembly and shape reconfigurable features. In contrast to pristine paraffin, the interconnected structure inside MTPCMs constitutes effective heat transfer pathways, coupling with high-thermal-conductivity NdFeB@Ag particles synergistically speed up the thermal charging/discharging rate, leading to 14~16 times enhancement in thermal conductivity for MTPCMs. Besides, MTPCMs display excellent compressive strength that is also attributed to their supporting architecture. In the end, we explore the application of MTPCMs in energy conversion and thermal management aspects, and the results reveal MTPCMs have superior energy conversion efficiency and temperature control capacity.

Results

MTPCMs and their features. As a basic unit in the 3D structure, the thermal conductivity of NdFeB particles will directly impact the heat transfer of MTPCMs. Considering this, we adopted in situ chemical plating method to coat a silver shell on the surface of micro NdFeB particles modifying them to NdFeB@Ag particles (details see Supplementary Fig. 1 and the “Method” section)[23]. As shown in Fig. 1b, the color of magnetic particles changed from dark black to yellow which was similar to the silver microparticles, indicating NdFeB particles are completely covered by silver shells. This was also demonstrated by scanning electron microscopy (SEM) images and the corresponding energy-dispersive X-ray spectroscopy (EDX) element mappings in Supplementary Fig. 2. In contrast to bare NdFeB, the core particle was wrapped in a continuous silver layer, and there existed only the silver element on the surface of NdFeB@Ag. The homogeneous composite of NdFeB@Ag particles and paraffin can be obtained by simply adding and stirring NdFeB@Ag particles into melted paraffin, correspondingly the resulting composite presented a yellow appearance (Fig. 1c). Applying a magnetic field to the composite, NdFeB@Ag particles aggregated forming a porous structure that provided the strong capillary force to stabilize paraffin, consequently the magnetically tightened form-stable phase change material (MTPCM) was born. The mixing ratio of NdFeB@Ag particles is an important parameter for MTPCMs as they compromise their energy storage density for the leakage-proof and form-stable abilities. It was explored that the lowest volume mixing ratio for MTPCMs was 15.84 %, and as a comparison, we prepared three samples with different volume ratios in this paper. Unless specified, the composite refers to the unmagnetized mixture of NdFeB@Ag particles and paraffin in the following context to facilitate elucidation.

It is deduced that MTPCMs have leakage-proof and shape stability behaviors based on the theoretical analysis. To verify this point, a leakage test was performed on the heating platform at 50°C for MTPCM, unmagnetized composite, and pristine paraffin, which were all processed into 10·10·10 mm cubes. As shown in Fig. 1d, after being heated for a while, pristine paraffine melted completely into a fluid spreading out on the plate. As for the unmagnetized composite, phase separation occurred during the phase change process, paraffin flowed away from the composite leaving a stack of collapsed NdFeB@Ag particles. Unlike the above two materials, no leakage was observed on the MTPCM block, and it always retained its initial shape even after being compressed by a weight of 20 g, which is ascribed to the magnetic-induced strong capillary force inside the material. The test result confirms the outstanding leakage-proof and shape stability capacity of MTPCMs. This conclusion was presented more vividly by hung the three samples and heated them through a heat gun. During the phase change process, the paraffin and unmagnetized composite melted and dropped on the table while the MTPCM was always hung on the string with its original shape (see Supplementary Movie 1).

Hard magnetic particles can reassemble and then rebuild an interconnected framework when their original structure is destroyed by external stimuli, which enables MTPCMs a shape transformable function. Only by a simple heating operation, the MTPCM transformed from cylinder to cuboid while maintaining its leakage-proof ability intact (Supplementary Movie 2). This function makes it convenient

to create or reconfigure MTPCMs to diverse geometries according to the specific application. Moreover, we fabricated MTPCMs into standard modules to make better use of their magnetism. The modules can attach spontaneously with good contact like “magnetic lego” due to the magnetic attraction. To further extend this concept, a series of intricate 3D architectures with different shapes and structures were realized via the modular assembly, and the generating object displayed a robust structure (Fig. 1e and Supplementary Movie 3). The above conformal shape and modular assembly features render MTPCMs favorable as they make instantly customize the shape of PCMs to meet complex practical requirements a reality.

The microstructure of the transverse section for MTPCMs was investigated using SEM and EDX. The cross-section images in Fig. 2a presented an oriented structure that is derived from the directional alignment of NdFeB@Ag particles and the accompanying passively arrayed paraffin. The anisotropic tendency in structure inevitably brings anisotropy performance to some extends. Besides, there were almost no voids inside the MTPCM, which is beneficial to its thermal and mechanical performance. The X-ray diffraction (XRD) pattern of the MTPCM in Fig. 2b only contained peaks of paraffin and pure Ag since the NdFeB particles are completely covered by silver shells. The XRD test states that NdFeB@Ag particles and paraffin is a physical combination and there is no new substance formed, revealing the force to stabilize paraffin is merely from magnetic-induced capillary action. To explore the magnetic properties of MTPCMs, we measured their magnetic hysteresis loops and surface magnetic flux density, as displayed in Fig. 2c-d. With the increase of volume ratio for MTPCM samples, their saturation magnetization and remanence rose from 50.22 to 58.72 emu g^{-1} and 32.81 to 38.15 emu g^{-1}, illustrating the MTPCMs have a good magnetic response and strong magnetism. Furthermore, a typical sample with the 19.12 % volume ratio was tested at different temperatures at different time points. The magnetic hysteresis loops tested at 20, 30, and 40°C on day 1 and day 30 almost overlapped. Even though the magnetic loops of the sample had a smaller enclosed area at 50°C, the values of saturation magnetization and remanence were nearly the same as those at other temperatures, which were about 54 and 35 emu g^{-1}. It is attributed to the high Curie temperature of NdFeB (315°C) that protect the magnetism of MTPCMs from high temperature. The results prove that MTPCMs own stable magnetism, which will not be affected by heating or long-time storage. The strong magnetism correspondingly generates high surface magnetic flux density in MTPCMs. For a 10·10·10 mm cubic MTPCM sample, the magnetic flux density on the surfaces which are parallel and perpendicular to the magnetic field reached up to 16.58 and 31.01 mT, respectively. Except for that, Fig. 2f shows the surface magnetic field profiles of MTPCMs with different shapes by magnetic observation cards. The samples all appeared a uniform magnetic field distribution and unambiguous boundary with their surroundings. The series of magnetic tests disclose MTPCMs have not only strong and stable magnetism but also homogeneous magnetic distribution without any defects.

Thermal and mechanical performance of MTPCMs. The phase change properties of MTPCMs were characterized by differential scanning calorimetry (DSC) (Fig. 3a). The curves of pristine paraffin and MTPCM samples with different volume ratios were very close, and the thermal parameters were extracted

and summarized in Fig. 3b. The onset melting and solidifying point of paraffin were 38.65 and 36.23°C, respectively. The three MTPCM samples had nearly the same values with paraffin (38.95 and 37.33°C for 15.84 %, 39.5 and 37.13°C for 19.12 % and 40.05 and 37.07°C for 23.31% sample). The fusion enthalpy for neat paraffin was 163.75 J cm^{-3}, as the addition of NdFeB@Ag particles, the value didn't decrease but instead changed to 178.70, 172.59 and 141.63 J cm^{-3}, which was ascribed to the magnetic particles increased the density of MTPCMs and thus improved their energy storage density. Moreover, unmagnetized composites were also measured by DSC and it was found that they had little difference with MTPCMs under the same volume ratio (Supplementary Fig. 3). These results indicate paraffin functions the dominant energy storage role in MTPCMs. The NdFeB@Ag particles only serve as the supporting material, and their magnetism does not affect the phase change characteristics of paraffin. Fig. 3c depicts the thermal gravimetric analysis (TGA) curves of paraffin and MTPCMs. Based on the data analysis, it can be achieved that the 5 % weight loss temperature of MTPCM was higher than that of paraffin, and this temperature boosted with the increase of volume ratio in MTPCMs. On the contrary, the weight loss rate declined with the addition of NdFeB@Ag particles. It is speculated that the capillary pores inside MTPCM protect paraffin from evaporation to some degree and finally delay its decomposition. Hence, MTPCMs have better heat resistance and thermal stability than pristine paraffin. The heat charging/discharging rate and temperature-hold time of PCMs are significant issues concerning their applications and they can be assessed via the heating and freezing process[17, 24]. The experiment system is shown in Supplementary Fig. 4, therein the MTPCM sample was produced into a 20·20·20 mm cubic block and the temperatures were set at 20 and 50°C with a heating/freezing rate of 1 K min^{-1}. The heating-freezing process was cycled 10 times and the curves are shown in Fig. 3d. In a magnified period, it can be observed that the heat charging/discharging rate and temperature-hold time presented an inverse variation trend with the increase of volume ratio in MTPCMs. Specifically speaking, the sample with a larger volume ratio costs a shorter time to reach the equilibrium state in both heating and freezing processes, implying it has higher heat charging/discharging rate. And this results from the more NdFeB@Ag particles build better heat transfer pathways, accelerating the thermal storage and release efficiency of the sample. However, adding more NdFeB@Ag particles leads to the reduction of paraffin, and this will cut down the latent heat of the sample. Correspondingly, its phase change time, namely temperature-hold time, decreases. Hence, it needs to balance these two aspects of MTPCMs in practical applications. Notably, MTPCMs exhibited almost the same heat charging/discharging rate and phase change time in 10 cycles, signifying the outstanding thermal-cycle reliability and durability of MTPCMs. As an essential property of PCMs, the thermal conductivity of MTPCMs was studied and described in Fig. 3e. The interconnected 3D structure of MTPCM offers efficient thermal conduction routes inside the entity. As the elementary unit on this network, modified NdFeB@Ag particles possess a silver-like high thermal conductivity. Under the synergistic effect of the above two factors, the thermal conductivity of MTPCMs is greatly enhanced by one order of magnitude compared to organic paraffin (0.21 W m^{-1} K^{-1}), reaching 2.97, 3.11, and 3.41 W m^{-1} K^{-1} for three different volume ratio samples. As stated above, the MTPCMs exhibited an anisotropic structure. Given the heat transfer mechanism in MTPCMs, we investigated the thermal conductivity of MTPCMs in the direction of parallel and perpendicular to the

magnetic field (Fig. 3f). It was easy to find that MTPCMs had higher thermal conductivity along the magnetic field direction and the difference of thermal conductivity in these two directions slightly rose with the increase of volume ratio in the samples (0.61 W m^{-1} K^{-1} for 15.84%, 0.7 W m^{-1} K^{-1} for 19.12% and 0.76 W m^{-1} K^{-1} for 23.31% sample). The anisotropic thermal performance in MTPCMs is mainly caused by the anisotropy in the structure, and this effect is reinforced with the increase of volume ratio in MTPCMs.

Applying a magnetic field, both soft and hard magnetic particles will rotate and align eventually forming chains along with the magnetic flux profiles[25, 26]. The different point is soft magnetic particles collapse back into a pile of powders while hard magnetic particles can hold their configuration after removing the magnetic field. This characteristic arouses our inspiration to explore whether the alignment of NdFeB@Ag particles throughout the MTPCM can support the composite and strengthen its mechanical performance. On this background, the compression tests were conducted on the 10·10·10 mm cubic MTPCM modules (the measurement system is shown in Supplementary Fig. 5). We first performed the tests at different temperatures, and the results are depicted in Fig. 4a. At room temperature, MTPCMs displayed high compressive yield strength, and this capacity was reinforced with the increase of volume ratio in the sample. Yet at the temperature above the melting point of paraffin, the MTPCMs continuously deformed and were ultimately compressed into the flattened cuboid when subjected to the normal force, suggesting they have negligible compressive strengths at this moment. These can be observed from the state of typical compressed samples in the insets as well. The solid paraffin tightly around the NdFeB@Ag chains forming a protective layer that offers a lateral force when the sample is compressed by the normal force, which helps the magnetic chains keep their original direction and thus harvest a good compressive strength. Once the paraffin has melted, the magnetic chains lose this support and rapidly yield to the compression force. Therefore, the directional alignment of NdFeB@Ag particles together with the assistant of paraffin make MTPCMs gain excellent compressive strength. Remarkably, even though the paraffin melted at a high temperature, no leakage of the sample occurred throughout the whole compression process, proving the superior leakage-proof ability of MTPCMs again (Supplementary Movie 4). Additionally, the compressive strength in different directions was measured to survey the anisotropy in the mechanical performance of MTPCMs. As we expected, the sample had a better compressive strength in the direction parallel to the magnetic field, originating from the anisotropic structure of the MTPCM. Compared to conventional PCMs, MTPCMs possess good mechanical performance and this could broaden their application to the field of green building.

Energy conversion and storage of MTPCMs. Employing PCMs in the areas of solar energy utilization, heat recovery, and power supply and demand regulation is all due to their large latent heat endows them with great energy conversion and storage potentials[27, 28, 29]. Limited by the severe fluctuation of sunlight, the solar-thermal conversion system cannot support a persistent output. As a result, electric-thermal and thermo-electric conversion and storage systems have become promising alternatives[1, 4, 30]. On this occasion, we investigated the electricity-to-heat and heat-to-electricity conversion and storage performance of MTPCMs. As is known to all, organic paraffin is an insulator that is impossible to conduct

electricity. However, as shown in Fig. 5a, the electrical conductivity of three MTPCM samples was $1.69{\cdot}10^4$, $2.25{\cdot}10^4$ and $2.83{\cdot}10^4$ S m^{-1}, respectively. The values are among the conductivity of metal materials ($\sigma{>}10^3$ S m^{-1}), certifying MTPCMs are good conductors of electricity. To figure out the underlying mechanism of this change (from insulator to a good conductor), we adopted the control variable mode, measuring the electrical conductivity of unmagnetized composites and the post-magnetized mixture of NdFeB and paraffin, respectively. It was found that the latter material was insulated and the unmagnetized composites had lower electrical conductivities than MTPCMs (Fig. 5b). This result elucidates that the modified NdFeB@Ag particles is a dispensable term to enable MPTCMs to become conductive, and on this basis, the interconnected 3D structure strengthens this effect further improving the electrical conductivity of MTPCMs. The electrical properties of MTPCMs are far beyond a high electrical conductivity. As discussed above, after being heated, NdFeB@Ag particles can reassemble building a new structure when the previous one is destroyed. With this feature, MTPCMs kept conductive regardless of encountering any deformations during the phase change process (Supplementary Movie 5). Owning such outstanding electrical performance is profitable to the electric-thermal conversion and storage of MTPCMs, and this is confirmed by the following experiments. A voltage of 3 V was applied on the MTPCM to trigger its electro-heat conversion, and the current stayed at 0.27 A in the whole process. Based on the temperature evolution of the sample, it can be calculated that the phase change time lasted for about 61 s and the electricity-to-heat harvest efficiency of MTPCM was 78.45 %. Generally, the phase transition time is relatively long under low voltage and the heat dissipation from the sample to surroundings increases accordingly, leading to reduced efficiency[30]. Therefore, such high efficiency at a low voltage demonstrates the prominent electricity-to-heat conversion and storage capacity of MTPCMs. Besides, a thermal infrared test was also implemented to express the electro-thermal conversion performance of MTPCMs qualitatively (Fig. 5c). A power of 8.88 W was input to the heart-shaped sample, and it turned to about 65°C in a short time of 30 s, suggesting the excellent performance of MTPCMs in the electricity-to-heat conversion and storage aspect again.

As the other energy harvesting system, the heat-to-electricity conversion and storage is executed via two MTPCM samples and an in-between thermoelectric generator. Herein, the paraffin in MTPCMs was replaced by EBiInSn (eutectic alloy of Bi, In, and Sn) whose melting point is 60°C to amplify the temperature gradient between the hot and cold side. The commercial thermoelectric device was a semiconductor that can convert the heat in the MPTCM into electrical energy according to the principle of the Seeback effect[2, 27]. As the heat source, the MTPCM was heated until the EBiInSn therein was melted. On account of the magnetic attraction feature of MTPCMs, the thermoelectric generator was tightly clamped having close contact with both two ends. We connected the system as a power supply to a self-programmed Bluetooth chip creating a hygrothermograph that can sensitively monitor the temperature and humidity of the local ambient in real-time (see Fig. 5d and Supplementary Movie 6). The evolution of temperature about the hot and cold side in the system and the corresponding voltage and current versus time are recorded in Fig. 5e. It can be seen that the MTPCMs made a high and long-lasting temperature difference, and accordingly, the power supply duration was over 4 min, and the maximum voltage and current reached 0.39 V and 0.13 A. To sum up, a 4.47 J net electrical energy was harvested from a small

MTPCM block (size: 20·20·10 mm). These data suggesting the large latent heat and superior heat-to-electricity conversion and storage performance of MTPCMs.

Thermal management of MTPCMs. Being identified as an important application branch, thermal management demands PCMs master high thermal conductivity, large latent heat, and appropriate phase transition temperature at the same time, which are what exactly our MTPCMs highlight[31, 32]. On top of that, most PCMs need containers and binders to prevent leakage and help them stick to the heat source[33, 34, 35]. However, introducing extra several layers between the PCM and heat source increases the thermal resistance, combing the binders are usually organic materials with extremely low thermal conductivity, the temperature control effect of PCMs will be greatly weakened. But for MTPCMs, this problem can be easily solved via their leakage-proof capacity and magnetism, as shown in Fig. 6a, two MTPCM blocks can directly attract to each other clamping the heat source between them with compact contact, which not only excludes the containers or binders between objects but also minimizes the interface contact resistant through close contact. To illustrate the thermal management capacity of MTPCMs, polyimide electric heating films were used as the heat source and they were sandwiched between two MTPCM and two paraffin blocks, respectively (Fig. 6b). The two structures were hung in the air to eliminate the influence of heat transfer between PCMs and the table. Unlike MTPCM blocks, it needed to drop some molten paraffin in the gap between two paraffin blocks to glue the heating film. When the electric heating films began to work, their temperature kept rising until reached the melting point of paraffin, from now on, the temperature of these two films went in different tendencies. Pure paraffin absorbed heat and melted to liquid, eventually felling off the heating film. While during this process, the MTPCM blocks were always attached to the film to absorb heat and held their shape unchanged (see Supplementary Movie 7). It can be seen from the temperature variations versus time that the two films presented the same temperature in the initial stage. From the transition point, the temperature of one film rose sharply, while the other film kept at about 40°C for 5.8 min, and afterward its temperature also rose slowly.

The above is the case that the heat source is not magnetic, if itself is a magnetic substance or plating a magnetic layer on the surface of the heat source, the MTPCM can directly attach to it to carry out thermal management. For instance, as represented in Fig. 6c, polyimide electric heating films stuck to the iron plates acting as the heat source. In virtue of the magnetism from the iron plates, the MTPCM block could directly contact the film for temperature control, and as a comparison, the other film didn't take any active heat dissipation steps. When the heating started, the temperature of the film without MTPCM rose rapidly reaching 65.33°C in 522 s under a power of 6 W, and once the power was cut off, its temperature dropped quickly to its beginning value (Fig. 6d). Overall, the temperature of the heat source fluctuated dramatically over a short period. But for the film using MTPCM block for thermal management, its temperature changed steadily and held at about 40°C for 43 s and 73 s in the heating and cooling section, respectively. This difference in temperature change for the two heating films can also be discovered intuitively by the sequential thermal infrared pictures. The aforesaid two experiments prove that MTPCMs have superb thermal management capacity and this arises from the combination of their good thermal properties and magnetism.

Batteries face a severe problem in practical application, that is, their performance is heavily dependent on the temperature[36]. Too high and too low temperature or even non-uniform temperature distribution will depress their energy and power capacity making batteries suffer from capacity fade and short lifespan[37, 38]. In this work, we engage MTPCMs for both heat dissipation at elevated temperature and low-temperature protection to regulate the working temperature of the flat-plate lithium-ion battery in a desirable range (Fig. 6e). The specific experimental details are recorded in the Methods section. When the battery discharged at a current of 17 A, its voltage dropped continuously until it reached the cut-off voltage at 168 s. While in this time the temperature increased slowly with the help of two MTPCM slices. It reached around 40°C after 96 s and stayed at this point for 16 s, then moved to the highest temperature of 41.75°C in the end. If the MTPCM slices were removed, for the same operation, the temperature in this process kept on rising and reached 60.85°C (Fig. 6f). It can be calculated that MTPCMs reduce the battery temperature rise by 31.39 % and this is attributed to the high thermal conductivity and large latent heat of MTPCMs. Towards the low-temperature situation, thanks to the excellent electrical properties, the MTPCM stripes can directly convert electricity to heat with high efficiency to warm up the battery from being frozen, forming an immediate protection scheme. In our experiment, the battery was cooled to -20°C by the incubator. Once the outer MTPCM stripes were powered on and the electric power of about 12.82 W was supplied to each stripe, the battery was heated up and its temperature rose to 46.07°C within 9.65 min. Even though the MTPCM stripes were powered off, the battery can still stay at the solidifying temperature of the MTPCM for 15 s and finally got a temperature of around 0°C through one heating operation (Fig. 6g). After the battery cooled down, we powered on the MTPCM stripes again and it can be seen that the battery presented almost the same temperature variation, suggesting the MTPCM slices own the cycling stability and can withstand the long and harsh working cycle conditions of the battery. The above heating and cooling experiments state that with prominent thermal performance and exclusive high electrical conductivity, MTPCMs have advantages in battery thermal management, they can control the battery temperature within normal values promptly, which is significant for high performance and long working time of the battery.

Discussion

Magnetism brings a strong binding force between magnetic particles. We utilize this effect and apply it to PCMs to solve their leakage issue. With this idea, the hard magnetic materials, NdFeB microparticles, were blended with paraffin. Given the low thermal conductivity of paraffin, NdFeB microparticles were firstly plated with a silver shell on their surfaces modifying them to NdFeB@Ag to enhance their thermal conduction. Through the magnetization operation, the NdFe@Ag particles aggregated and aligned along the magnetic field forming an oriented 3D porous structure and the paraffin was carried in the micropores between particles. The magnetic-induced tightly connected particles lead to strong capillary force, under this action, the paraffin is stabilized in the structure synthesizing unprecedented magnetically tightened form-stable phase change materials (MTPCMs). We studied and characterized this material thoroughly. It is found that the lowest volume ratio of NdFeB@Ag particles in MTPCMs is 15.84 % and as long as the particles are more than this critical value, MTPCMs will own leakage-proof ability and shape stability. The

directional alignment of NdFeB@Ag particles makes MTPCMs present strong magnetism, and standard MTPCM modules can assemble and reconfigure into diverse robust shapes via magnetic attraction. Besides, it can also through a simple heating operation to process MTPCMs into any shape while keeping the above abilities intact, and this is due to the interaction between magnetic particles as well. Hence, magnetism endows MTPCMs with magnetic assembly and conformal geometry features.

The 3D structure build by NdFeB@Ag particles is the base of MTPCMs, it not only lets MPTCMs attain leakage-proof and magnetism capacities but also improves the performance of these materials. In the thermal aspect, the NdFeB@Ag particles just function as the supporting material and have no impact on paraffin, thereby MTPCMs retain the proper melting/solidifying point and large latent heat. Except that, the magnetic particles protect paraffin from evaporation and decomposition to some extent, making MTPCMs possess better thermal stability. The interconnected structure provides heat transfer pathways, combined with the superior thermal conduction of NdFeB@Ag together enhancing the thermal conductivity of MTPCMs by 14~16 times than pristine paraffin. In addition, MTPCMs also exhibit efficient thermal storage/release and thermal-cycle reliability in the heat charging/discharging cycles. As for the mechanical aspect, unlike conventional PCMs, the supporting structure reinforces the compressive strength of MTPCMs. They can resist large compression force at room temperature, and even at the temperature above the melting point of paraffin, MTPCMs can still maintain the leakage-proof ability under compression. Furthermore, magnetic particles' head-to-tail alignment triggers an anisotropic structure and consequently brings about a slight anisotropy in thermal and mechanical performance for MTPCMs.

With the above excellent properties, we apply MTPCMs in energy conversion and thermal management to test their performance in practical applications. The 3D structure and silver shells of NdFeB@Ag also provide conduction paths for electricity, consequently causing MTPCMs to appear with a metal-like electrical conductivity. As a result, they behave high energy conversion efficiency and energy harvesting ability in the electricity and heat conversion. While in the temperature control area, MTPCMs own unique advantages. The leakage-proof capacity and magnetism of MTPCMs allow them to directly attach to the hot object for temperature control without using containers and binders, which greatly reduces the thermal resistance between PCMs and heat sources. On top of that, MTPCMs perform well in battery thermal management, they can offer both heat dissipation at elevated temperature and low-temperature protection for the battery, regulating its temperature in a stable range. In conclusion, introducing hard magnetic particles to PCMs proposing an innovative route to tackle the liquid leakage and low thermal conductivity issues of PCMs, and the accompanying-generated series of properties in PCMs make them preponderant in practical applications.

Methods

Materials. NdFeB microparticles were purchased from Magnequench International. LLC. Silver nitrate ($AgNO_3$) was bought from Aladdin Industrial Corporation. Polyvinylpyrrolidone (PVP, average molecular

weight=8000), D- Glucose, and ammonium hydroxide solution were provided by Macklin Biochemical Co., Ltd.

Characterizations and property measurements. SEM and EDX images were observed by QUANTA FEG 250. XRD patterns were tested using the Bruker D8 Focus X-ray diffractometer. Magnetic hysteresis loops were obtained by a cryogen-free cryocooler-based physical property measurement system (VersaLab) from Quantum Design Inc. The magnetization and demagnetization rate was set as 100 Oe s^{-1} with the magnetic field change of up to 30 kOe. The surface magnetic flux density was measured by Gaussmeter. DSC measurement was implemented on NETZSCH DSC 200F3 Maia equipment with a ramp rate of 10 K s^{-1}. TGA was conducted by NETZSCH TG 209F3 instrument with a heating rate of 10 K min^{-1} under the nitrogen atmosphere. Thermal conductivity was calculated by the equation $\lambda = a \cdot C_p \cdot \rho$, where a represents the thermal diffusivity, C_p is specific heat capacity, and ρ is density. The thermal diffusivity was measured by the NETZSCH LAF 467 instrument and density was acquired using the METTLER TOLEDO XSE105 analytical balance with XS/XP-Ana Density Kit. For specific heat capacity, it was tested by the abovementioned DSC equipment. The mechanical property of MTPCMs was measured using a universal testing machine (MTS-E45.105) equipped with an incubator, and the compression rate was set as 2 mm min^{-1} during the test. Electrical conductivity was measured by a standard four-point method. The sample was filled in a tailored groove, a voltage was applied and the resistance was measured by a micro ohmmeter (Agilent 34420A). The electrical conductivity was calculated using $\sigma = s/R \cdot l$, where s is the cross-sectional area, R is the resistance of the sample, and l is the length of the groove.

Surface modification of NdFeB. The surface modification of NdFeB to NdFeB@Ag was implemented by in situ chemical plating processing. Typically, weight ratios of several reagents were selected as NdFeB:$AgNO_3$=2:1, PVP: $AgNO_3$=1:1 and glucose:$AgNO_3$=2:1. Firstly, PVP together with NdFeB particles were added to adequate deionized water (DI). After PVP was thoroughly dissolved in DI, mechanical agitation was employed to the suspension for 20 min to make sure every NdFeB particle was covered by a PVP film. Then, the suspension was kept still for a few minutes and the supernatant was poured off to obtain the precipitated NdFeB particles. Next, the silver ammonia solution was prepared by dropping ammonia hydroxide in the $AgNO_3$ solution until it turned transparent, and NdFeB particles were resuspended in silver ammonia solution for the following plating process. The suspension was first mechanically agitated for 10 min and afterward, it was transferred to the heating platform. As the reductant of the reaction, glucose solution was produced by dissolving glucose in DI. Since the optimum temperature of the silver plating reaction was above 60°C, until the suspension was heated to a relatively high temperature, glucose solution was added and the mechanical agitation was turned on. During the reaction, it can be observed that the suspension became yellow slurry in a short time indicating the successful reduction of silver ions. The silver plating reaction was done in about 15 min and the synthesized NdFeB@Ag particles were extracted, rinsed, and dried in a vacuum oven.

Preparation of MTPCMs. NdFeB@Ag particles can be easily dispersed in melted paraffin by manually stirring. To fabricate MTPCMs, a tailored rectangle mold with an electrical heating function was used to

keep the composite liquid during the magnetization process, which enables NdFeB@Ag particles to rotate and align along the magnetic field. The mold filled with the composite was placed on the sample stage and a magnetic field with 2 T magnetic flux density was exerted to the composite for 30~60 s. After magnetization, the heating function was turned off and a moderate pressure was applied to the MTPCM until it solidifies. The pressure could eliminate the porosity in MTPCMs, which is a common issue in composite materials. For as-prepared MTPCMs, they can be processed to standard modules by a wire cutting machine.

Thermal management of battery

The commercial flat-plate lithium-ion battery had a nominal capacity of 950 mAh, a nominal voltage of 3.2 V, and a maximum continuous discharge rate of 20 C. To obtain a better electro-heat conversion effect, the MTPCM was fabricated to a stripe with 5 mm width·1.5 mm thickness·20 mm length. Then the stripe was designed to be embedded in a 60·50·3 mm matrix with a serpentine shape to acquire uniform temperature distribution in the heating/cooling process. The matrix was a mixture consisting of NdFeB particles and paraffin. Since the phase change material in matrix and stripe was both paraffin and paraffin was stabilized by magnetism in the two materials, the as-prepared slices were called MTPCM slices. The MTPCM slices can attract each other clamping the battery between them to implement the heating and cooling experiment. As shown in Supplementary Fig. 7, the battery was discharged by a battery testing system in the cooling process, and the MTPCM stripes were heated by electricity in the heating process.

Declarations

Acknowledgments: The authors would like to acknowledge the National Natural Science Foundation of China (NSFC) (Grant No.52076213), and the 2115 Talent Development Program of China Agricultural University, and the NSFC Key Project (Grant No.91748206) for the financial coverage of this work.

Author contributions: Y.L. and D.Y. contributed equally to this work. Y.L. and D.Y. designed and conducted the experiments. J.L. and Z.H. supervised the investigations. H.D. did lots of work in the preliminary experiment. J.L. programmed the hygrothermograph system. H.Z. performed the magnetic characterization. L.C. helped with the sample fabrication. Y.L. drafted the manuscript with inputs from all other authors. All the authors agreed on the final manuscript.

Corresponding author: Correspondence to Zhizhu He and Jing Liu. Email: zzhe@cau.edu.cn and jliu@mail.ipc.ac.cn.

Competing interests: The authors declare no competing interests.

Data availability: All relevant data generated or analyzed during this study are available in this published article and its supplementary information files, or from the corresponding authors upon reasonable request.

References

1. Wu MQ, Wu S, Cai YF, Wang RZ, Li TX. Form-stable phase change composites: Preparation, performance, and applications for thermal energy conversion, storage and management. *Energy Storage Materials* **42**, 380–417 (2021).
2. Yuan K, *et al.* Engineering the thermal conductivity of functional phase-change materials for heat energy conversion, storage, and utilization. *Advanced Functional Materials* **30**, (2019).
3. Gerkman MA, Han GGD. Toward Controlled Thermal Energy Storage and Release in Organic Phase Change Materials. *Joule* **4**, 1621–1625 (2020).
4. Yang J, *et al.* High-performance composite phase change materials for energy conversion based on macroscopically three-dimensional structural materials. *Materials Horizons* **6**, 250–273 (2019).
5. Chen X, Tang Z, Liu P, Gao H, Chang Y, Wang G. Smart utilization of multifunctional metal oxides in phase change materials. *Matter* **3**, 708–741 (2020).
6. Wang W, *et al.* Electromagnetic and solar energy conversion and storage based on Fe3O4-functionalised graphene/phase change material nanocomposites. *Energy Conversion and Management* **196**, 1299–1305 (2019).
7. Kashyap V, *et al.* Full Spectrum Solar Thermal Energy Harvesting and Storage by a Molecular and Phase-Change Hybrid Material. *Joule* **3**, 3100–3111 (2019).
8. Qiu L, Ouyang Y, Feng Y, Zhang X. Review on micro/nano phase change materials for solar thermal applications. *Renewable Energy* **140**, 513–538 (2019).
9. Farid MM, Khudhair AM, Razack SAK, Al-Hallaj S. A review on phase change energy storage: materials and applications. *Energy Conversion and Management* **45**, 1597–1615 (2004).
10. Ge H, Li H, Mei S, Liu J. Low melting point liquid metal as a new class of phase change material: An emerging frontier in energy area. *Renewable and Sustainable Energy Reviews* **21**, 331–346 (2013).
11. Kenisarin M, Mahkamov K. Solar energy storage using phase change materials. *Renewable and Sustainable Energy Reviews* **11**, 1913–1965 (2007).
12. Wu S, *et al.* High-performance thermally conductive phase change composites by large-size oriented graphite sheets for scalable thermal energy harvesting. *Adv Mater* **31**, e1905099 (2019).
13. Min P, *et al.* Thermally conductive phase change composites featuring anisotropic graphene aerogels for real-time and fast-charging solar-thermal energy conversion. *Advanced Functional Materials* **28**, (2018).
14. Wang Z, *et al.* Dynamic tuning of optical absorbers for accelerated solar-thermal energy storage. *Nat Commun* **8**, 1478 (2017).
15. Qiu J, Huo D, Xia Y. Phase-Change Materials for Controlled Release and Related Applications. *Adv Mater* **32**, e2000660 (2020).
16. Salunkhe PB, Shembekar PS. A review on effect of phase change material encapsulation on the thermal performance of a system. *Renewable and sustainable energy reviews* **16**, 5603–5616 (2012).

17. Yu D-H, He Z-Z. Shape-remodeled macrocapsule of phase change materials for thermal energy storage and thermal management. *Applied Energy* **247**, 503–516 (2019).
18. Zhao CY, Wu ZG. Heat transfer enhancement of high temperature thermal energy storage using metal foams and expanded graphite. *Solar Energy Materials and Solar Cells* **95**, 636–643 (2011).
19. Zhao L, Xing Y, Liu X. Experimental investigation on the thermal management performance of heat sink using low melting point alloy as phase change material. *Renewable Energy* **146**, 1578–1587 (2020).
20. Li A, *et al.* Network structural CNTs penetrate porous carbon spport for phase-change materials with enhanced electro-thermal performance. *Advanced Electronic Materials* **6**, (2020).
21. Yang J, *et al.* An ice-templated assembly strategy to construct graphene oxide/boron nitride hybrid porous scaffolds in phase change materials with enhanced thermal conductivity and shape stability for light–thermal–electric energy conversion. *Journal of Materials Chemistry A* **4**, 18841–18851 (2016).
22. Yang J, *et al.* Hierarchically interconnected porous scaffolds for phase change materials with improved thermal conductivity and efficient solar-to-electric energy conversion. *Nanoscale* **9**, 17704–17709 (2017).
23. Zheng R, *et al.* A novel conductive core–shell particle based on liquid metal for fabricating real-time self-repairing flexible circuits. *Advanced Functional Materials* **30**, (2020).
24. Zhou D, Yuan J, Zhou Y, Liu Y. Preparation and characterization of myristic acid/expanded graphite composite phase change materials for thermal energy storage. *Sci Rep* **10**, 10889 (2020).
25. Kuang X, *et al.* Magnetic Dynamic Polymers for Modular Assembling and Reconfigurable Morphing Architectures. *Adv Mater* **33**, e2102113 (2021).
26. Goudu SR, Yasa IC, Hu X, Ceylan H, Hu W, Sitti M. Biodegradable Untethered Magnetic Hydrogel Milli-Grippers. *Advanced Functional Materials* **30**, (2020).
27. Yu C, Yang SH, Pak SY, Youn JR, Song YS. Graphene embedded form stable phase change materials for drawing the thermo-electric energy harvesting. *Energy Conversion and Management* **169**, 88–96 (2018).
28. Tao P, *et al.* Magnetically-accelerated large-capacity solar-thermal energy storage within high-temperature phase-change materials. *Energy & Environmental Science* **12**, 1613–1621 (2019).
29. Liu H, *et al.* Optically triggered synchronous heat release of phase-change enthalpy and photo-thermal energy in phase-change materials at low temperatures. *Advanced Functional Materials* **31**, (2020).
30. Chen L, *et al.* Electro- and Photodriven Phase Change Composites Based on Wax-Infiltrated Carbon Nanotube Sponges. *ACS Nano* **6**, 10884–10892 (2012).
31. Shamberger PJ, Bruno NM. Review of metallic phase change materials for high heat flux transient thermal management applications. *Applied Energy* **258**, 113955 (2020).

32. Ling Z, *et al.* Review on thermal management systems using phase change materials for electronic components, Li-ion batteries and photovoltaic modules. *Renewable and Sustainable Energy Reviews* **31**, 427–438 (2014).
33. Kenisarin MM, Kenisarina KM. Form-stable phase change materials for thermal energy storage. *Renewable and Sustainable Energy Reviews* **16**, 1999–2040 (2012).
34. Fukahori R, Nomura T, Zhu C, Sheng N, Okinaka N, Akiyama T. Macro-encapsulation of metallic phase change material using cylindrical-type ceramic containers for high-temperature thermal energy storage. *Applied Energy* **170**, 324–328 (2016).
35. Browne M, Norton B, McCormack S. Phase change materials for photovoltaic thermal management. *Renewable and Sustainable Energy Reviews* **47**, 762–782 (2015).
36. Liu K, Liu Y, Lin D, Pei A, Cui Y. Materials for lithium-ion battery safety. *Science Advances* **4**, eaas9820.
37. Hu X, Zheng Y, Howey DA, Perez H, Foley A, Pecht M. Battery warm-up methodologies at subzero temperatures for automotive applications: Recent advances and perspectives. *Progress in Energy and Combustion Science* **77**, (2020).
38. Wu W, Wang S, Wu W, Chen K, Hong S, Lai Y. A critical review of battery thermal performance and liquid based battery thermal management. *Energy Conversion and Management* **182**, 262–281 (2019).

Figures

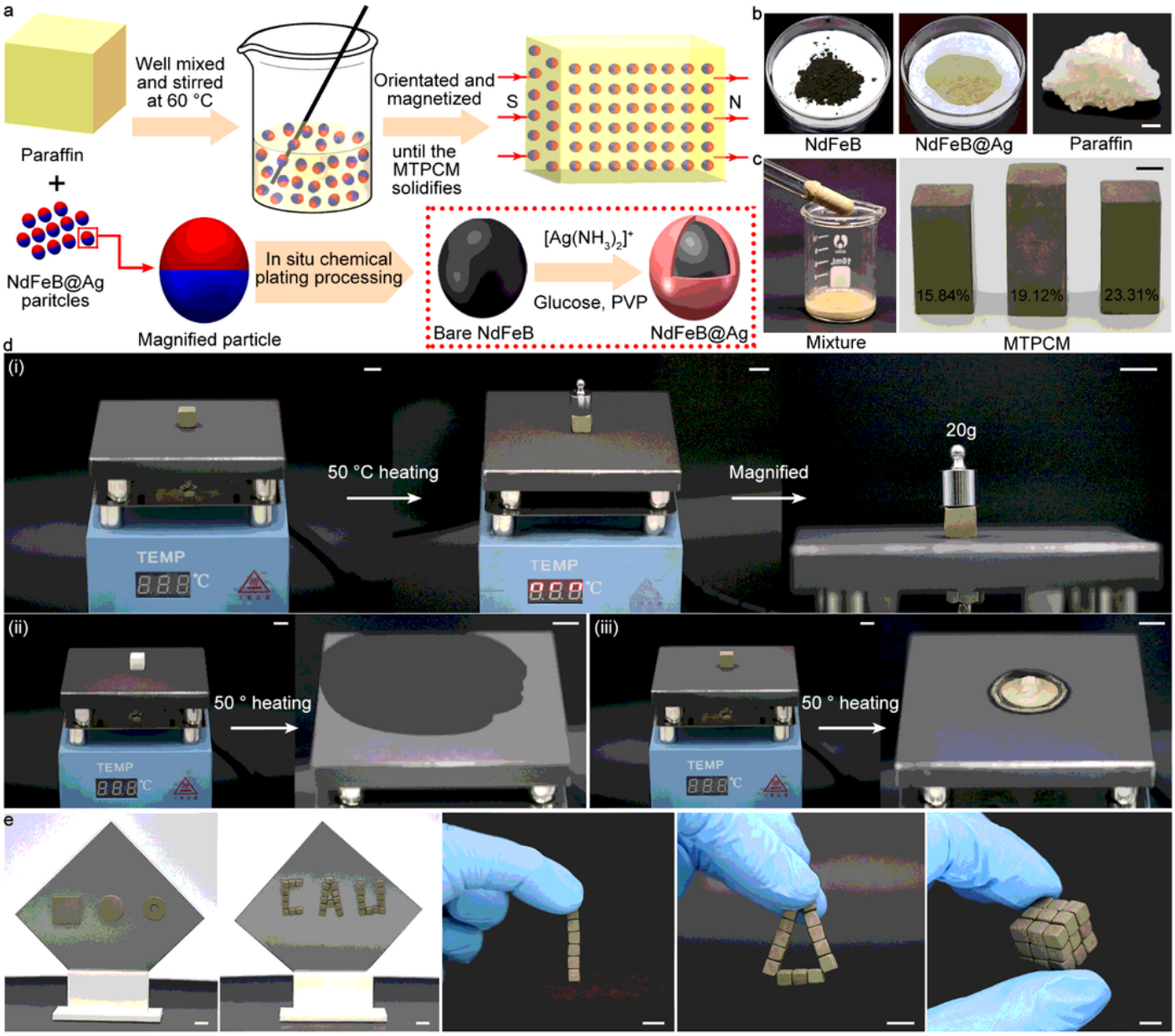

Figure 1

MTPCMs with magnetic assembly and conformal shape features. a Schematic procedure for fabricating MTPCMs. b Photographs of NdFeB, NdFeB@Ag, and paraffin. Scale bar: 5 mm c The mixture of NdFeB@Ag particles and paraffin, and MTPCMs with different volume ratios. Scale bar: 5 mm. d Shape stability and leakage behaviors of (i) MTPCM (ii) paraffin and (iii) unmagnetized composite during the

phase change process. Scale bars: 10 mm. e Modular assembly and conformal geometry features of MTPCMs. Scale bars: 10 mm.

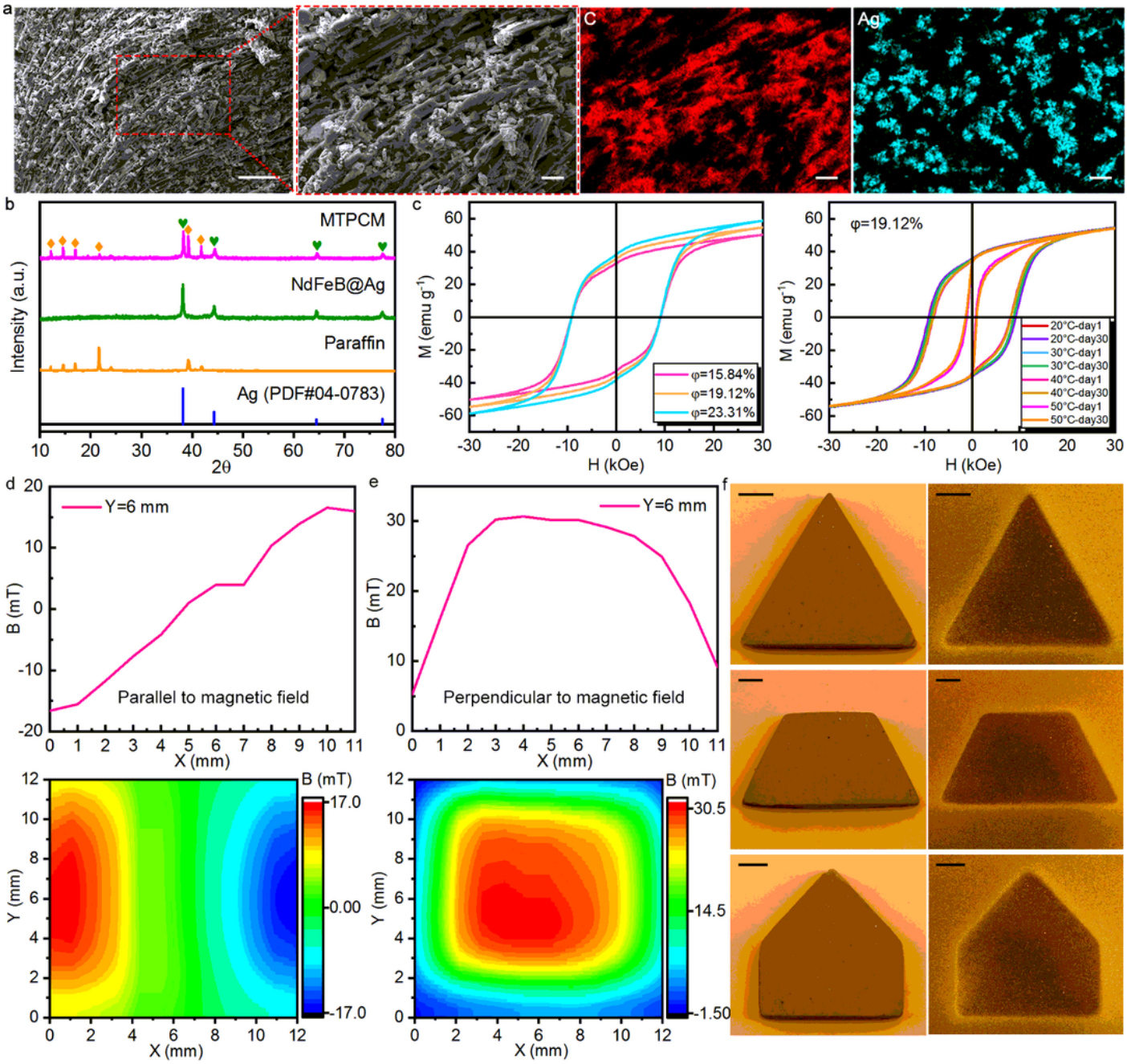

Figure 2

Characterizations of MTPCMs. a SEM images and the corresponding EDX element mappings for the cross-section of MTPCMs, revealing the directional alignment of NdFeB@Ag particles induced by the magnetic field. Scale bars: 50 μm, 10 μm, 10 μm and 10 μm. b Comparison of XRD patterns among

MTPCM, NdFeB@Ag, paraffin, and the PDF card of pure Ag. c Magnetic hysteresis loops of MTPCMs with different volume ratios and the typical MTPCM sample at different temperatures at different time points. d,e Surface magnetic flux density of MTPCM in the direction along and perpendicular to the magnetic field. f Surface magnetic field distributions of MTPCMs with different shapes. Scale bars: 4 mm.

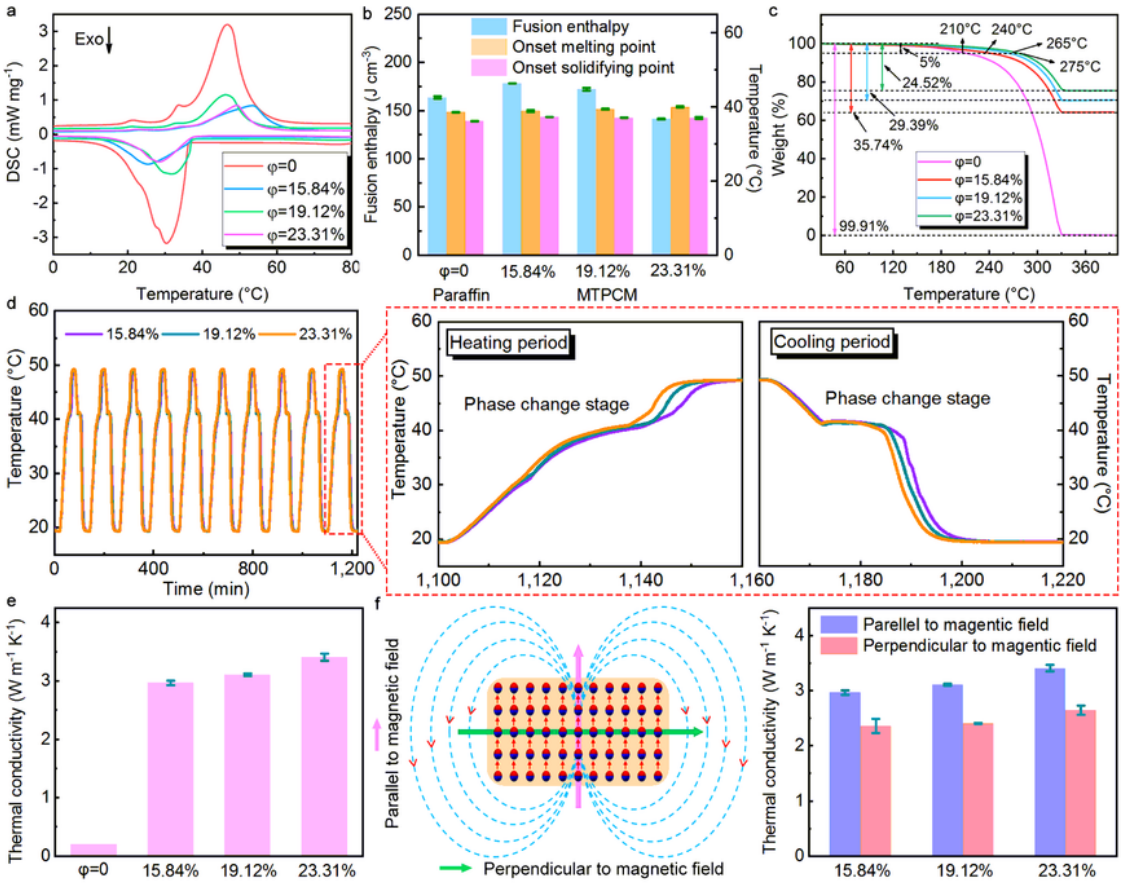

Figure 3

Thermal performance of MTPCMs. a DSC curves of paraffin and different volume ratio MTPCMs. b Comparison of fusion enthalpy, onset melting, and solidifying point of pristine paraffin and MTPCMs with different volume ratios. c TGA curves of paraffin and different volume ratio MTPCMs. d Temperature variations of MTPCM during the heat charging/discharging cycles and the magnified heating-freezing process in one period. e Thermal conductivities of pristine paraffin and MTPCMs with different volume ratios. f Schematic diagram of the directional alignment of NdFeB@Ag particles in paraffin matrix and the consequently anisotropic thermal conductivities of MTPCMs.

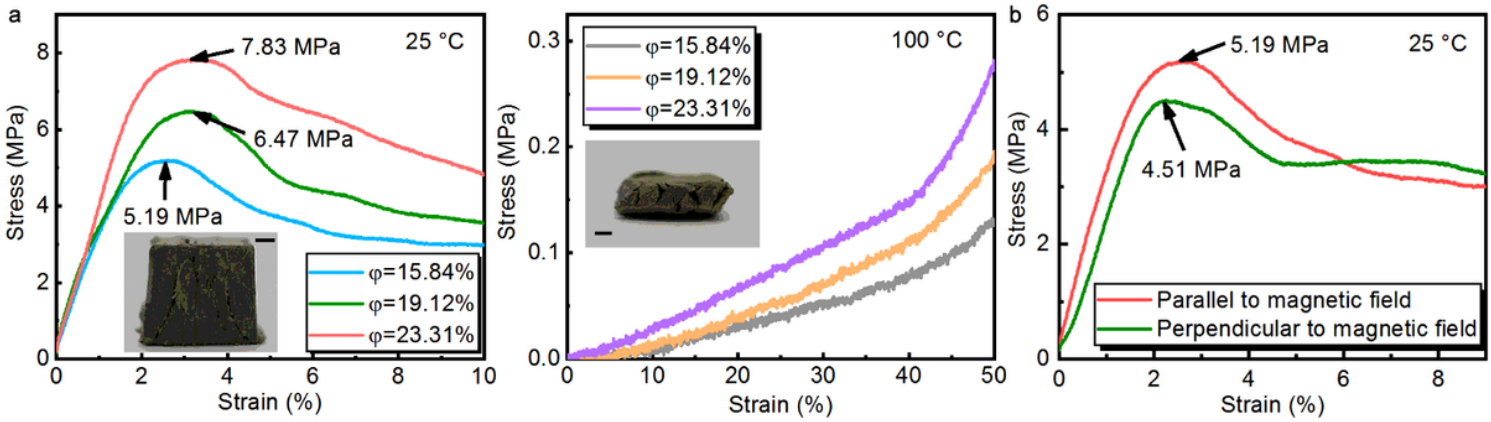

Figure 4

Mechanical performance of MTPCMs. a Compression stress-strain curves of MTPCMs at temperatures below and above the melting point. The insets are the typical compressed samples. Scale bars: 2mm. b Anisotropic compression stress-strain curves of MTPCM at different directions.

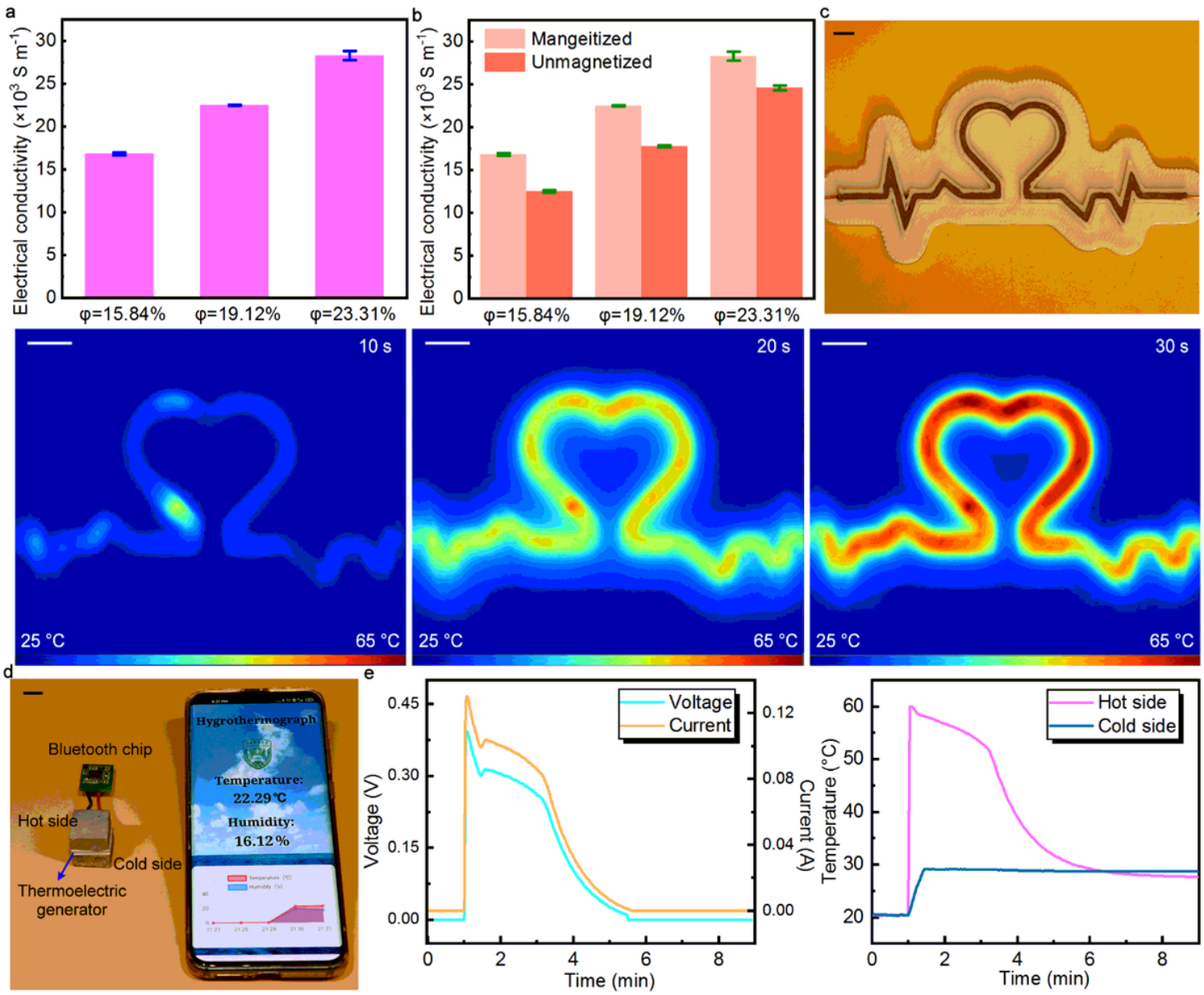

Figure 5

Energy conversion and storage applications of MTPCMs. a Electrical conductivities of MTPCMs with different volume ratios. b Electrical conductivities of MTPCM and unmagnetized composites. c Photo and thermal infrared images of MTPCMs during the electricity-to-heat conversion process. Scale bars: 5 mm. d Photo of the heat-to-electricity conversion and storage system. Scale bar: 10 mm. e Output voltage and current, and temperature evolution curves of the heat-to-electricity conversion and storage system.

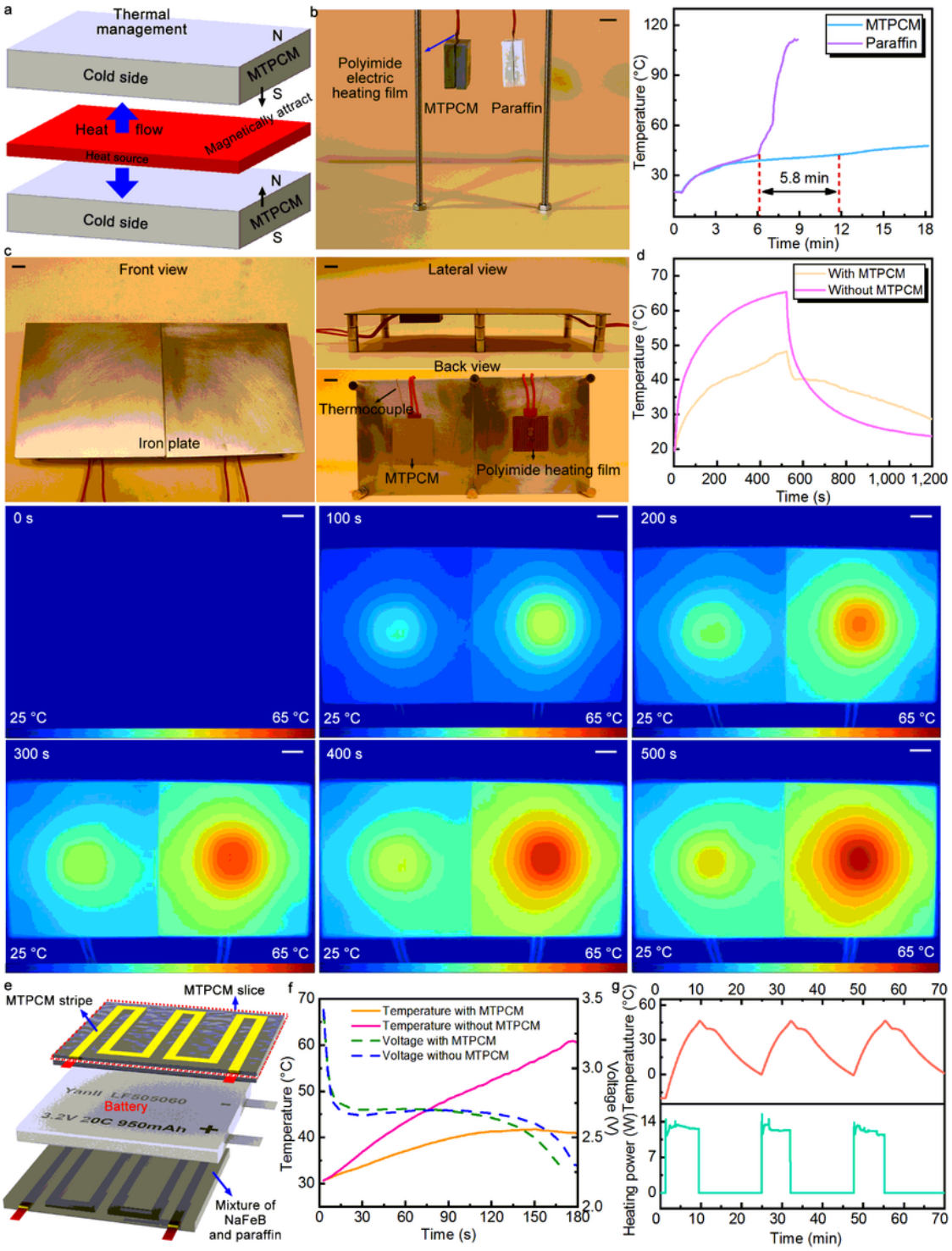

Figure 6

Thermal management applications of MTPCMs. a Schematic diagram of MTPCM blocks applied to the temperature control of nonmagnetic heat source. b The corresponding photo and temperature evolution of MTPCM and paraffin blocks. Scale bar: 10 mm. c Photos about the temperature control of MTPCM on the magnetic heat source. Scale bars: 1 cm. d Temperature evolution and the corresponding thermal infrared images of the heat source with and without the MTPCM. Scale bars: 5 mm. e Schematic

illustration of battery thermal management system. f Temperature and voltage evolution of lithium-ion battery during the discharging process. g Temperature variation of the battery and the heating power of one MTPCM slice under the low-temperature protection situation.

Supplementary Files

This is a list of supplementary files associated with this preprint. Click to download.

- SupplementalInformation.pdf
- Movie5.mp4
- Movie3.mp4
- Movie4.mp4
- Movie6.mp4
- Movie1.mp4
- Movie2.mp4
- Movie7.mp4